JOURNAL OF MATERIALS SCIENCE **40** (2005) 3969–3980

Microstructural and electrical resistance analysis of laser-processed SiC substrates for wide bandgap semiconductor materials

I. A. SALAMA*
Intel Corporation -Assembly Technology Development, 5000 W Chandler Blvd., CH5-159, Chandler, Arizona 85226-3699

N. R. QUICK
Applicote Associates, 894 Silverado Court, Lake Mary, Florida 32746

A. KAR
Laser-Aided Manufacturing, Materials and Micro-Processing Laboratory (LAMMMP), School of Optics, Center for Research and Education in Optics and Lasers (CREOL), University of Central Florida, Orlando, Fl 32816-2700.
E-mail: akar@creol.ucf.edu

Highly conductive phases have been generated on different polytypes of SiC substrates using a laser direct-write technique. Incorporation of both *n*-type and *p*-type impurities into the SiC substrates was accomplished by laser irradiation in dopant-containing ambients. X-ray diffraction, energy dispersive X-ray spectroscopy, and X-ray photoelectron spectroscopy have been used to detect the presence of the dopant atoms and the compositional variation induced by laser irradiation. Scanning electron microscopy was used to study the microstructure, morphology and dimensions of the converted regions. The conversion in electric resistance has been attributed to both structural and compositional variations observed for the irradiated tracks

1. Introduction

Silicon carbide is the only tetrahedral compound known to be formed by the IVB group elements in the periodic table. As many other close-packed materials, SiC exhibits a one-dimensional type of polymorphism known as polytypism. While SiC crystallizes mainly in three lattice structures (cubic, hexagonal and rhombohedral), more than 200 different polytypes are known to exist for SiC with the exact physical properties of each type being dependent on the crystal structure [1]. The polytypes are similar within the closest-packed planes (basal planes) and are different in the stacking direction normal to these planes. The stacking sequence, expressed by the ABC notation, describes the alternative arrangements of the different atomic layer. Here, each letter represents a bilayer of individual Si and C atoms. The ABCA. . .. stacking sequence resulted in the zinc blend crystal structure where each SiC bilayer can be oriented only into three different positions with respect to the lattice point while maintaining the sp^3-bonding configuration of the SiC [2]. This particular arrangement is known as 3C-SiC or the β-phase, where 3 refers to the number of the Si/C bilayers needed for the periodicity, and it is the only possible polytype of SiC in the cubic structure. When the stacking sequence is ABA, the crystallographic symmetry is hexagonal (Wurtzite) and the material is known as 2H-SiC. All other polytypes are intermixed forms of both the hexagonal and the cubic symmetries. One defines hexagonality, H, as the fraction of two-layer stackings that are hexagonal out of all the possible cubic and hexagonal stackings, i.e., $\mathrm{H} = h/(h + c)$ where h and c are the numbers of hexagonal and cubic stackings, respectively. Two most common polytypes of this category are 4H-SiC and 6H-SiC where the overall symmetry is hexagonal with stacking sequence of ABCBABCB and ABCACBABCACB, respectively [3]. The 6H-SiC is composed of one-third hexagonal bonds and two-third cubic bonds while the 4H-SiC has an equal contribution of the hexagonal and cubic bonding configurations. All the non-cubic polytypes are collectively known as α-SiC [4].

Different polytypes of silicon carbide have different physical and electronic properties. At room temperature, 3C-SiC has the lowest bandgap energy ($E_g \approx 2.4$ eV) with very high electron mobility, second to 4H-SiC ($E_g \approx 3.02$ eV). The hole mobility (μ_h) and electron mobility (μ_e) are important parameters that affect

* This work was performed while he was at the University of Central Florida, Orlando, Florida.

the device performance [5], *e.g.*, the direct proportion between the transconductance, g_m, and the carrier mobility in field effect transistor (FET) devices. The ratio of the electron mobility in the basal plane ($\mu_{//}$) to that along the normal to these planes ($\mu_{\perp}$) is about 1.25 and 0.16 for 4H-SiC and 6H-SiC polytypes, respectively. Due to this anisotropic property of 6H-SiC, 4H-SiC polytype is the first choice in microelectronic device applications [4].

Compared to other wide bandgap semiconductor materials, SiC is the fastest emerging candidate for applications where high operating temperature, high-power, -frequency, -switching speed, and radiation hard microelectronic devices are needed [6]. SiC is superior to the conventional semiconductor materials (Si, Ge and GaAs) in many aspects that are crucial for integrated device design. The bandgap energy in silicon carbide ($E_g = 2.36$ to 3.5 eV) [7] is three times that of Si and GaAs, and more than five times that of Ge. The electric field breakdown strength of SiC (3–5 MV/cm) is typically six times that of Si. Despite its higher electric field strength, the saturation electron velocity ($v_{\text{sat}} \approx 2 \times 10^7$ cm/s) in SiC is similar to that in GaAs. Excellent thermal conductivity of SiC (350–490 W m^{-1} K^{-1}), which is three times higher than silicon and seven times higher than GaAs [7, 8], allows silicon carbide to remove heat more efficiently, operate at lower internal junction temperature and therefore the cooling hardware is reduced for SiC devices.

To fully utilize the above-mentioned electrical and thermal properties of SiC for high temperature and high power applications, some fabrication building blocks (*n*-region, *p*-region, and heavily doped channels) must be established. Historically, the fabrication of a defect free SiC substrate has been the most difficult step limiting the utilization of SiC in microelectronic industries. Various techniques can be used for SiC growth, *e.g.*, melt-growth, physical vapor deposition (PVD) and chemical vapor deposition (CVD). The requirements of high temperature ($T > 3000^\circ$C) and high pressure ($P > 10^5$ atm) to obtain a stoichiometric melt and the solvent (Si) evaporation problem at $T > 1750^\circ$C exclude the melt-growth technique as a viable method to grow SiC crystals. PVD via seeded sublimation has been the most investigated and widely used technique to produce SiC boules where the vapor phase of SiC (Si, Si_2C, SiC_2) is deposited on a SiC seed crystal at a high temperature ($T > 2000^\circ$C). Commercial fabrication of 3-inch diameter SiC wafers by using this technique has been reported [9]. Different arrangements are possible in the CVD method. One technique is to use silane and propane gases as precursors to grow SiC on a graphite substrate, where the growth temperature is in the range of 1500–1700°C and the precursors are diluted in hydrogen carrier gas.

Low diffusion coefficient of most impurities in SiC [10], and the hardness, chemical inertness and high bond strength of SiC eliminate the use of conventional diffusion techniques for doping SiC. Ion implantation and epilayer doping are the two most widely used techniques for doping SiC substrates. In the latter case, in-situ doping is accomplished during the CVD epitaxial growth through the introduction of *N* for *n*-type and Al for *p*-type epilayers [11]. Other dopants such as phosphorous (P), boron (B), and vanadium (V) can be used for *n*-type, *p*-type, and semi-insulating epilayers, respectively. The production of defect free and semi-insulating SiC substrates is extremely important to produce electronic and optoelectronic devices [12]. Recent development in the epilayer doping includes the use of the site-competition technique in which certain dopant species can be either excluded or heavily introduced into the growing SiC crystal by varying the Si to *C* ratio in the reactant gas. SiC epilayer with dopant concentration ranging from 9×10^{14} to 1×10^{19} atoms/cm^3 is commercially available with a high doping uniformity (4% variation in the dopant concentration over 30 mm wafer) for both *n*-type and *p*-type substrates [13].

Ion implantation is another technology for doping SiC substrates which requires high temperature treatment of the substrate to achieve acceptable implantation and electrical activation of the dopant [14, 15]. Most of the ion implantation processes are carried out in the temperature range 600–800°C using a patterned high temperature masking material and then the mask is stripped to anneal the substrate at a much higher temperature (1400–1800°C) to maximize electrical activation of the dopant. For *n*-type implants, both nitrogen and phosphorus are widely used elements due to their low ionization energy and the ease of electrical activation in SiC. Al, B, and Ga are used for *p*-type implants in SiC. The main challenges in the case of *p*-doping are higher ionization energy for the *p*-dopants than for the *n*-dopants, out-diffusion at high temperature annealing especially in the case of B [15] and damage-assisted sublimation etching of SiC, *i.e.*, selective loss of silicon from the SiC surface upon annealing [16]. Co-implantation of carbon with *p*-type dopant has been investigated as a means of improving the electrical conductivity of implanted *p*-type contact layer [15, 17]. One of the disadvantages of ion implantation in SiC is the generation of defect centers [18]. Dopant implantation in compound semiconductors such as SiC alters the stoichiometry of the substrate by changing the atomic ratio of Si to C near the SiC surface, and thereby affects further implantation [18, 19]. One of the current challenges in ion implantation is the requirement of high ion energy to obtain a deep level junction and the associated lattice damage that increases with the implantation energy. For a deep level *p*-type implant, B is preferred to Al because Al can cause more lattice damage due to its higher atomic mass. Also high temperature implantation is preferred to room temperature implantation since the latter can cause amorphization to the substrate while the former does not.

A laser conversion technology, first reported by Quick as the laser direct-write technique [20, 26], was used by Sengupta *et al.* [27] to generate conductive tracks on an insulating SiC substrate surface without requiring any metallization. The laser direct-write process alters the electric properties of SiC thin films and bulk substrates significantly (*e.g.*, resistivity decreases from 10^{11} to 10^{-4} Ω·cm) and this conversion is stable at high temperatures [26]. Sengupta *et al.* [27]

also demonstrated laser metallization and fabricated a Schottky diode on a SiC substrate using the laser-direct write technique. The electrical property conversion, selective-area doping, post-doping treatment by using the direct-write technique and the effect of various processing parameters were reported by Salama *et al*. [28]. The present paper reports microstructural and compositional changes in laser-irradiated samples. The electric resistance conversion in various laser-treated samples and the effect of different process parameters on the extent of this conversion are discussed. Different analytical techniques are used to understand the mechanism of the observed electric resistance conversion in SiC samples. Precise controllability, ease of computer automation to direct a laser beam and its localized intense heating capability make the laser direct-write technique advantageous over the conventional methods for processing wide bandgap materials.

2. Experimental studies

Three types of samples: black color polycrystalline sintered α-SiC (6H-SiC) samples (2.5 mm thick) processed by a pressureless sintering thermal treatment cycle, black color CVD β-SiC (cubic SiC) wafers (0.20 mm thick) and greenish 4H-SiC low-doped epilayer wafers (0.25 mm thick) are considered in this study. Laser-irradiation experiments were conducted using a Nd:YAG laser source of wavelength (λ) 1064 nm that can be operated in both continuous wave (CW) and Q-switched modes. The incident laser power was varied from 10 to 170 W for the experiments with the CW lasers. In the case of Q-switched mode, the pulse repetition rate was varied from 1 to 35 kHz. The laser was operated in these two modes due to the different optical properties of these samples requiring different amounts of laser irradiance at the substrate surface to induce electric resistance changes in each case. The sintered α-SiC samples were laser-treated in the CW mode, while the 4H-SiC samples were laser-treated in the Q-switched mode.

A schematic of the laser-direct writing and doping system is shown in Ref. [28]. The SiC sample is placed inside a gas-tight $10 \times 10 \times 10$ cm^3 plexiglass chamber with a soda-lime glass window for laser beam delivery. Laser-irradiated tracks were formed on the sample surface by moving the chamber on a stepper motor-controlled translation stage at different speeds referred to as laser scanning speeds. The height of the chamber was controlled manually through an intermediate stage to obtain different laser spot sizes on the SiC substrate surface. The laser scanning speeds were 0.8, 1 and 5.6 mm/s for various results presented in this paper. For electrical property conversion, experiments were conducted keeping the sample in an argon atmosphere ($P = 0.1$ MPa). N-type tracks were formed in a nitrogen atmosphere ($P = 0.1$ MPa) and insulating tracks were created in an oxygen environment at a pressure of 0.1 MPa. Trimethylaluminum (TMA) was used as a precursor to incorporate Al into SiC. TMA was separately heated in a glass flask till it evaporates and then a carrier gas (Ar) was passed through the flask to deliver the TMA vapor to the laser processing chamber using a gas-tight tube.

Four-probe resistance measurements were carried out at room temperature using an HP3478A multimeter with a resolution of $\pm 1\Omega$ and $\pm 10\ \Omega$ in 30 Ω and 300 kΩ ranges, respectively. The probes were made of copper wire having 0.5 mm tip diameter. The transmission of electromagnetic radiation in the CVD β-SiC and 4H-SiC wafers was measured using a spectrophotometer in the wavelength range $\lambda = 200$ to 3000 nm. The reflected power from the sintered α-SiC sample was measured as a function of the incident laser power using a power detector.

X-ray diffraction patterns were obtained for powder samples using Cu K_α radiation in the angular range ($2\theta = 10$–105°) with a step size of 0.02° and a scanning speed of 0.6° per min.

Noran Voyager 2 instrument, which is a scanning electron microscope (SEM) equipped with energy dispersive X-ray spectroscopy (EDS), was used to analyze the samples. The EDS was run at an accelerating voltage 15 keV, working distance 15 mm, take-off angle 90° and X-ray signal acquisition time 150 s for all the samples discussed in this paper. The calculated elemental atomic concentration was based on the ZAF correction method involving 24 oxygen atoms and 6 iterations as a standard in the Noran Voyager 2 instrument. The error in the elemental analysis was 0.1 wt% in the case of Si and Al and 0.8 wt.% for C and N. The chemical composition and bonding states for both the laser-treated and as-received samples were studied by X-ray photoelectron spectroscopy (XPS) using a monochromated Al K_α source and a cylindrical mirror analyzer for the spectrometer. The spectrometer was calibrated using Au ($4f_{7/2}$) = 84 eV and Ag ($4d_{5/2} = 368.3$ eV). Each of the XPS spectra was acquired from 30 repeated sweeps.

3. Results and discussion

The above-mentioned studies allowed analysis of the opto-thermal effects, microstructural and compositional changes in laser processing of SiC.

4. Opto-thermal analysis

The laser power absorbed by the sintered α-SiC sample is plotted in Fig. 1 as a function of the incident laser power at $\lambda = 1064$ nm. At the incident power $P = 80$ W (the critical value of the laser power at which conversion in electric resistance was observed for the sample irradiated in argon) [28], the reflectance (R) is about 0.18 which is close to the value ($R = 0.17$) measured by Spitzer *et al*. [29] for the C-face of a 6H-SiC single crystal. This value of the reflectance ($R = 0.18$ at $P = 80$ W) was then used to calculate the maximum temperature at the laser beam center on the α-SiC substrate surface as a function of the incident power using the following expression [30, 31] for a scanning speed of 1 mm/s, and is plotted in Fig. 1.

$$T(0,t) = \frac{2I_a}{k}\sqrt{\frac{\alpha t}{\pi}} \tag{1}$$

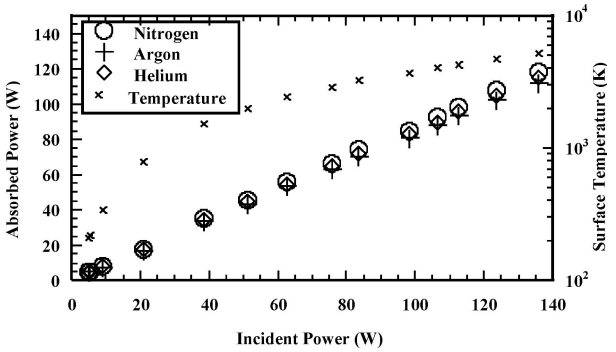

Figure 1 The absorbed power Vs. the incident power for the sintered α-SiC irradiated with CW Nd:YAG laser in different ambients (beam diameter = 1 mm, CW mode at room temperature). Also illustrated is the surface temperature calculated as a function of the incident power for the sample.

Here $T\,(0,\,t)$ is the substrate surface temperature at the laser beam center, t is the laser-substrate interaction time which is defined as $t = v/d$ for CW laser processing where v is the laser beam scanning speed and d is the laser beam spot diameter at the substrate surface. I_a is the absorbed power density given by $\frac{4P}{\pi d^2}(1-R)$, k is the thermal conductivity and α is the thermal diffusivity of the substrate. The values of k and α were taken for the 6H-SiC polytype, *i.e.*, 4.9×10^2 W/m K and 2.2×10^{-4} m^2/s, respectively [7], since the samples were found to contain this polytype substantially as evident from XRD analysis that will be discussed below.

The transmission spectrum of the 4H-SiC wafer (green color) is shown in Fig. 2a indicating that minimum transmission (10%), *i.e.*, maximum absorption, occurs at $\lambda \approx 480$–490 nm. This is consistent with the green color appearance of the wafer. The transmission increases to a peak at $\lambda \approx 700$ nm and then it decreases to 40%, i.e., the absorption is about 60%, at the wavelength of Nd: YAG laser ($\lambda = 1064$ nm). The maximum transmission occurs at $\alpha = 850$ nm in the case of the β-SiC wafer (Fig. 2b) and the sample exhibits almost 100% absorption in the visible range which is consistent with the black color appearance of the sample.

5. X-ray diffraction (XRD) for phase identification

The X-ray powder diffraction pattern of the untreated sintered α-SiC sample is presented in Fig. 3a, showing that most of the diffraction lines are identical to those of the 6H-SiC polytype with the presence of excess carbon phase ($2\theta \approx 26^\circ$) and two small peaks of the 5H-SiC polytype at $2\theta \approx 100$–102° [32]. The X-ray pattern of the laser argon-treated sample is presented in Fig. 3b showing that laser treatment increases the relative intensity of the free carbon peaks at $2\theta \approx 26^\circ$. It also shows two other small peaks at $2\theta \approx 50^\circ$ and 65° corresponding to the diamond cubic silicon phase [33]. It can be seen in Figs 3a and b that the Si peak at $2\theta \approx 65^\circ$ coincides with one of the 6H-SiC peaks [32, 33]. Since all other SiC peaks do not increase in intensity upon irradiation, the increase in the relative intensity of the diffraction peak at $2\theta = 65^\circ$ is attributed to the Si phase instead of the SiC phase. The relative intensity of the 2H-graphite peak in the irradiated sample is much higher than that of the untreated sample [34]. The diffraction pattern of the laser nitrogen-treated α-SiC sample is presented in Fig. 3c showing that all of the SiC peaks, except the peak at $2\theta \approx 35.7^\circ$, are substantially reduced in intensity. At the angular positions $2\theta \approx 26$–27°, the deconvolution of the diffraction lines revealed the presence of two different peaks for the laser nitrogen-treated sample instead of a single line observed in the laser-argon treated sample (see inserts in Figs 3b and c, respectively). The positions of the peaks were 26.519° and 26.616° for the nitrogen-treated sample. These two lines were fitted to those of hexagonal nitrogen [34] and 2H-graphite [35] phases, respectively. The diffraction pattern does not show any silicon nitride peaks in the laser nitrogen -treated sample because the main peak of the silicon nitride phase that should occur at $2\theta \approx 27.05^\circ$, 33.6° and 36.05° with relative intensities 100%, 99% and 93%, respectively, were absent [36]. This suggests that laser-irradiation of SiC in a nitrogen-containing environment favors the incorporation of nitrogen into the SiC lattice to the formation of silicon nitride or carbo-nitride compounds.

6. X-ray photoelectron spectroscopy (XPS) for laser-treated surface analysis

XPS analysis was conducted to study the effect of Q-switched Nd:YAG laser irradiation on the surface chemistry of 4H-SiC single crystal wafer (Figs 4a–c). The ratios of the carbon to silicon signal intensities obtained from the core level spectra of C 1s, Si 2s and Si $2p^{3/2}$

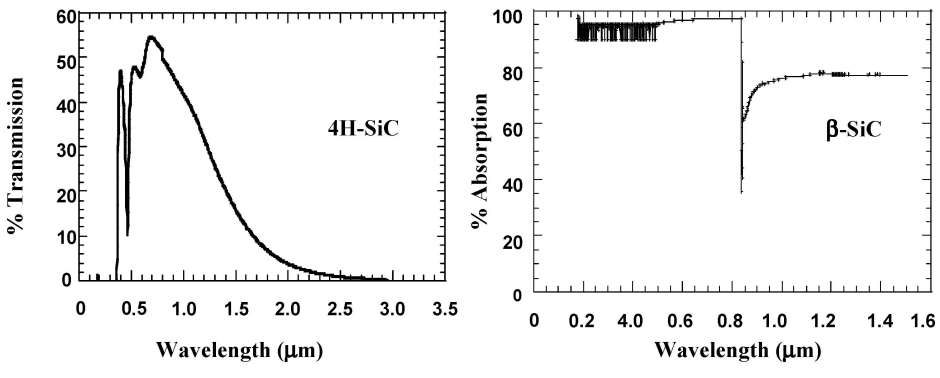

(a) Single crystal green 4H-SiC wafer **(b) CVD black β-SiC wafer**

Figure 2 Transmission and absorption spectra showing the optical responses of two types of SiC substrates.

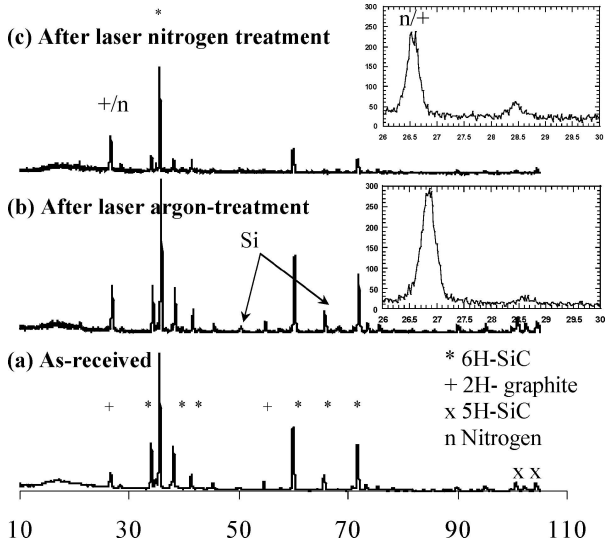

Figure 3 X-ray powder diffraction patterns for (a) as-received (b) laser-argon irradiated (c) laser-nitrogen irradiated, sintered α-SiC samples. For the patterns shown in b and c the irradiation was performed using Nd:YAG laser, CW mode, beam spot diameter =1 mm, scanning speed = 1 mm/s. Gas pressure = 0.1 MPa for both nitrogen and argon.

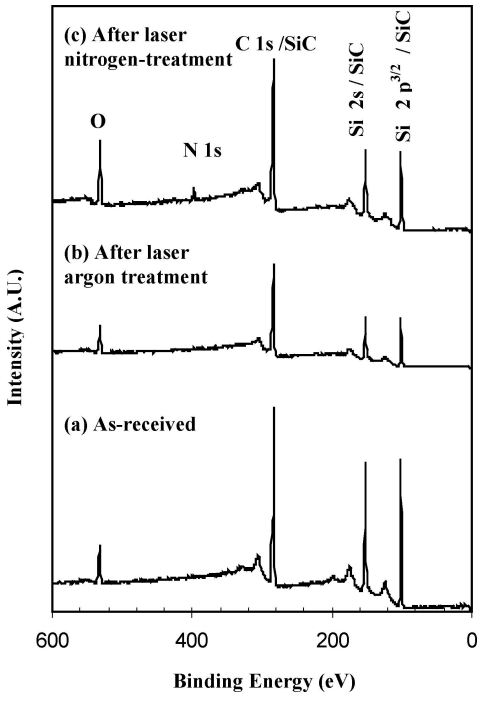

Figure 4 XPS spectra of the 4H-SiC single crystal wafer (a) in the as received condition (b) after laser irradiation in argon (c) after laser irradiation in nitrogen. For samples in b and c the irradiation was performed using Nd:YAG laser beam spot diameter = 1 mm. The laser runs in a Q-switch mode at pulse repetition rate = 2.0 kHz, pulse width = 0.6 ns. pulse energy = 2.8 mJ, scanning speed = 5.6 mm/s.

are listed in Table I. While laser irradiation in argon increases the *C* to Si ratio for the two silicon signals, 2s and $2p^{3/2}$ as shown in Fig. 4b, laser irradiation in nitrogen increases the C to Si ratio more than that observed in the argon-treated sample and leads to the presence of a nitrogen signal (N 1s at 397 eV) as shown in Fig. 4c. The XPS spectrum of the laser nitrogen-treated sample confirms the results of the XRD pattern shown in Fig. 3c, where the incorporation of nitrogen into the SiC substrate has been demonstrated.

TABLE I The ratio of carbon to silicon (C/Si) signals' intensities for the XPS spectra shown in Fig. 4

Sample	(C 1s/ Si 2s)	(C 1s/ Si $2p^{3/2)}$
Untreated sample	1.379	1.340
Laser treated in argon	1.994	2.00
Laser treated in nitrogen	2.060	2.12

Figs 5a–c compare the Si $2p^{3/2}$ core level signals in the SiC spectra of the as-received, laser argon-treated and laser nitrogen-treated 4H-SiC wafers, respectively. In the Si $2p^{3/2}$ spectra, the laser irradiation in argon has shifted the Si-C peak slightly from 101.5 eV of the as-received sample (Fig. 5a), to a lower energy value (Fig. 5b). After laser irradiation in argon, a weak signal was observed at 98.9 eV corresponding to the binding energy of silicon. The irradiation in nitrogen caused overlapping of the Si-C and Si signals and broadened the Si-C peak around 101 eV (Fig. 5c). The extensive broadening of the Si-C signal for the nitrogen-treated sample makes it difficult to detect the presence of any Si-N signal that is typically present in bulk SiN_x samples at 101–102 eV depending on the value of x that represents the exact stoichiometry of the silicon nitride phase ($x = 0.3$–1.3). However, the broadening in the lower binding energy side (Fig. 5c) suggests that the number of Si-Si bonded states has increased in the laser nitrogen-treated sample compared to the laser argon-treated one.

The C 1s spectra for the as-received, laser argon-treated and laser nitrogen-treated samples are shown in Figs 5d–f, respectively. Laser irradiation in argon broadens the C-Si peak at 282.7 eV towards the higher binding energy side and causes it to slightly overlap on the C═C signal at 285.4 eV. Irradiation in nitrogen did not create the C═N (286.1 eV) and C─N (287.5 eV) bondings that are typically observed in CN_x films. Instead, it broadened the C─Si peak (Fig. 5f) preferentially towards the higher binding energy side overlapping it on the C═C signal at 285.5 eV. Fig. 5g presents the N 1s core spectra for laser nitrogen-treated sample showing that the binding energy of the incorporated nitrogen is closer to the N─Si bond than to the N─C bond, which indicates that the N─Si bonding is more likely to occur than the N─C bonding. The N─N and N─O signals at 402.2 eV are very small indicating that these bonds are not formed.

The presence of the Si peak in the Si $2p^{3/2}$ spectra and the overlap between the C═C and C─Si in the C 1s spectra (Fig. 5e) suggest that laser irradiation decomposes a certain amount of SiC into Si and C at the substrate surface. This also agrees with the XRD results (Fig. 3b) where the graphite peak intensity increases and the free silicon peaks appear due to laser irradiation in argon. The C 1s and N 1s spectra indicate that the formation of Si─N is favored compared to the C─N bonding during laser nitrogen treatment. This means that nitrogen is more likely to occupy the C sites in the SiC lattice owing to the similar atomic radii of N and C atoms.

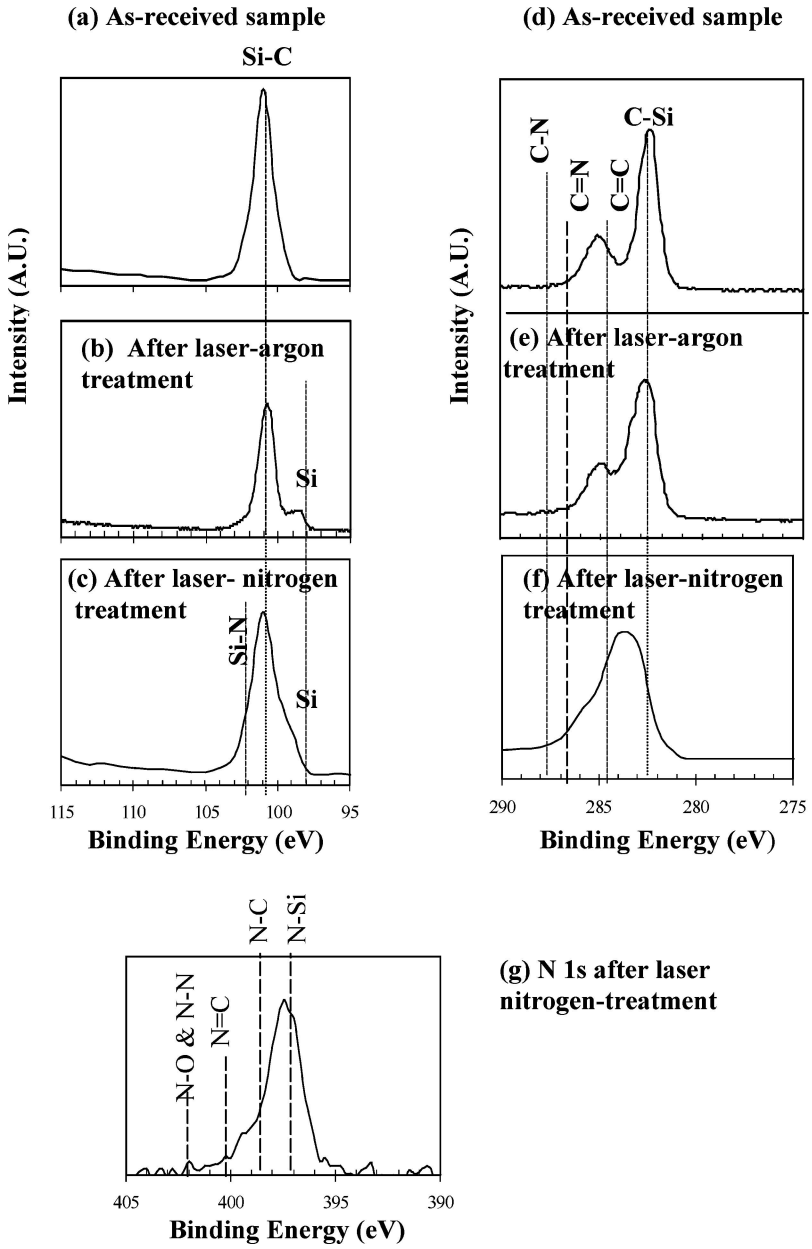

Figure 5 The effect of laser irradiation on; Si $2p^{3/2}$ [shown in (a, b, c)], C 1s [shown in (d, e, f)] and N 1s [shown in (g)] signals in the XPS spectra of the 4H-SiC wafers.

7. Scanning electron microscopy (SEM) for microstructural analysis

Scanning electron microscopy (SEM) was used to obtain secondary emission micrographs (Fig. 6) for the sintered α-SiC sample laser-treated in argon and nitrogen with a CW Nd:YAG ($\lambda = 1064$ nm) laser of power 80 W, beam diameter 1 mm and scanning speed 1 mm/s, and gas pressure 0.1 MPa. The morphology of the irradiated region is nonuniform across the laser beam scanning direction. The variation in the track morphology could be due to several reasons. A multimode laser beam was used in this study. Discontinuous intensity distribution in such a beam can cause localized heating and melting of the substrate leading to the observed variation in the morphology. The second reason may be due to the formation of periodic patterns frequently observed in high energy laser processing [37], which is due to the interference between the incident laser and the diffracted electromagnetic waves. Different models have been proposed to explain the formation of such periodic patterns [37–39].

Figs 6c and d represent higher magnifications of the central regions a1 and b1 of the laser-treated tracks in argon and nitrogen environments, respectively, showing the formation of carbon-rich globules. The formation of these globules at the track center is due to the following reasons. The SiC substrate surface temperature, calculated by using Equation 1, for an incident laser power of 80 W is higher than the SiC peritectic reaction temperature $T_p \approx 2540^{\circ}$C [2]. Under equilibrium conditions, the peritectic reaction of SiC yields two phases: liquid silicon with 27 at% dissolved carbon and a solid carbon phase. Due to short laser-matter interaction time, fast heating and rapid solidification in laser processing, the thermal and chemical conditions in the laser-melted pool may deviate from the equilibrium state. The short laser-substrate interaction time and the nonuniform power distribution in the laser beam will

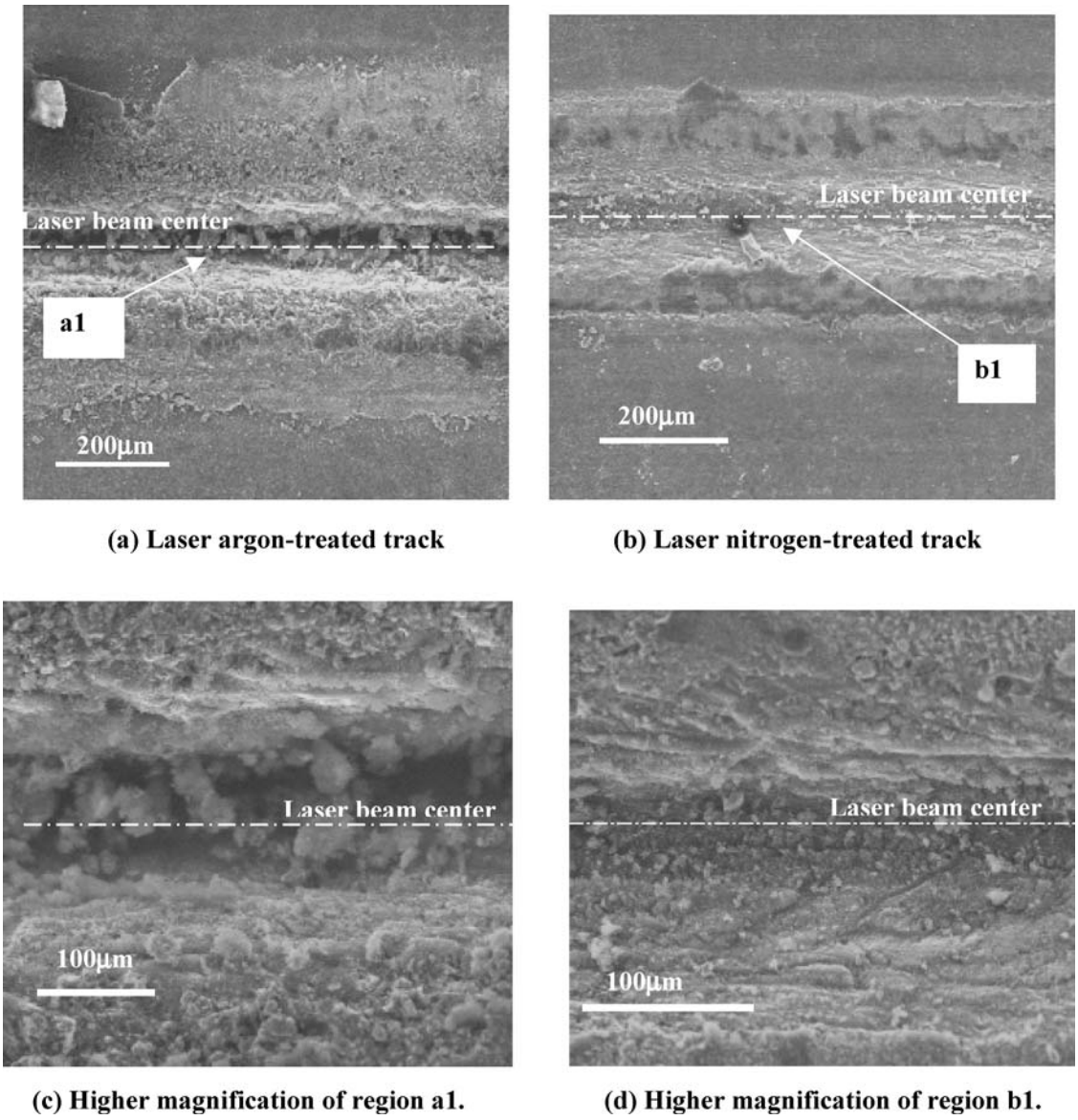

Figure 6 SEM micrographs of a sintered α-SiC sample after laser irradiation in two different environments. Laser power 80 W in CW mode, beam diameter = 1 mm, scanning speed = 1 mm/s, and gas pressure = 0.1 MPa.

cause nonuniform heating resulting in molten Si with dissolved C, free C and unmelted SiC in the melt pool. This melt pool solidifies rapidly causing less segregation of the solute (carbon) atoms. Under such nonequilibrium conditions, the reaction products are unmelted SiC, resolidified silicon with carbon content larger than 27 at% and free carbon phases. It should also be noted that higher vapor pressure of Si than that of SiC [7], and high surface temperature due to laser irradiation will selectively vaporize silicon which will assist in the formation of carbon-rich globules as observed at the laser track center.

The globules are finer and more uniformly distributed in the case of nitrogen treatment than in the case of argon treatment as illustrated in Figs 6c and d. This may be because nitrogen enhances the decomposition of SiC into liquid Si with dissolved nitrogen and carbon, and unmelted SiC particles (Table I). The enhanced decomposition reduces the amount of unmelted SiC particles in the melt pool, which means fewer sites are available for heterogeneous nucleation. Therefore, most of the carbon-rich liquid silicon will solidify via homogeneous nucleation resulting in uniformly distributed small size globules.

While the sintered α-SiC samples (Fig. 6) were laser-treated in the CW mode, the laser treatment in the case of 4H-SiC wafer (Fig. 7) was performed with a Q-switched Nd:YAG laser ($\lambda = 1064$ nm) of beam diameter 1 mm, pulse repitition rate 2 kHz, pulse width 70 ns, pulse energy 0.7 mJ and scanning speed 0.8 mm/s, and gas pressure 0.1 MPa. Due to different absorptivities of these two types of samples, different laser processing conditions were selected to induce microstructural changes in the samples via laser heating mechanisms in order to examine the effects of laser heating on microstructural changes in these two types of samples. Two SEM micrographs of a laser-treated 4H-SiC wafer are presented in Fig. 7 showing different microstructures compared to those observed for the sintered α-SiC sample (Fig. 6). The surface of the carbon-rich phase at the center of the irradiated track is flatter and smoother in the case of 4H-SiC sample (Fig. 7a) than in the case of the 6H-SiC samples (Figs 6a and b). The region A, which is about 50 μm away from the laser beam center

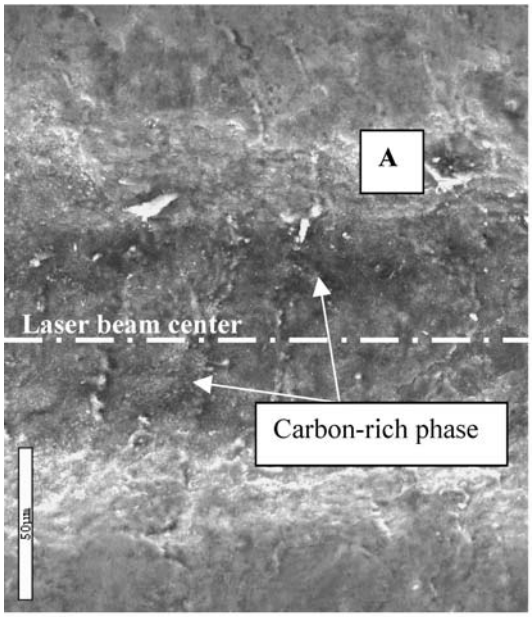

(a) Region near the center of the laser irradiated track

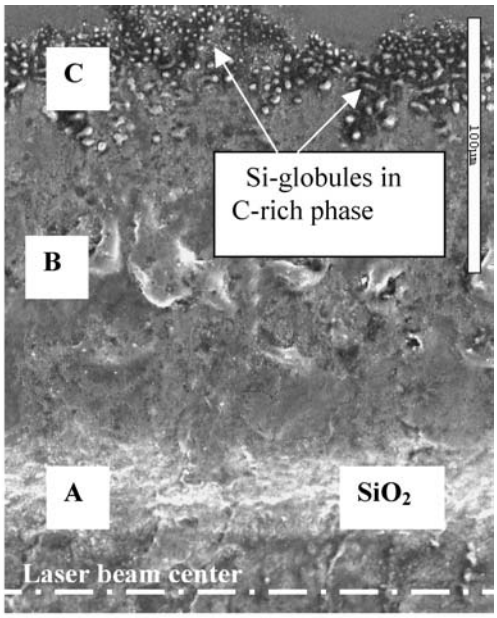

(b) Region near the interface between the irradiated track and the wafer's original surface. Regions B and C are not shown in Fig. 7a since they are relatively far away from the laser beam center in the lateral direction and therefore, outside the micrograph.

Figure 7 SEM micrographs of single crystal 4H-SiC surface after laser irradiation in argon atmosphere. Laser beam diameter 1 mm, Q-switched mode, pulse repitition rate = 2 kHz, pulse width = 70 ns, pulse energy = 0.7 mJ, scanning speed = 0.8 mm/s, and gas pressure = 0.1 MPa.

in Fig. 7a, contains a large amount of SiO_2. The morphology of region B, which is about 100 μm away from the beam center (Fig. 7b), is quite similar to that at the beam center shown in Fig. 7a. Higher magnification of region *C*, which is about 200 μm away from the beam center, is shown in Fig. 8a where the white globules represent an almost pure silicon phase that is surrounded by a dark carbon-rich phase. These two phases are denoted by *Y* and *X*, respectively, in Fig. 8a. The size of the silicon globules is in the range of 0.2–2.0 μm, much smaller than that of the carbon globules observed at the beam center of the laser-treated 6H-SiC samples (Figs 6c and d). The formation of such a highly segregated microstructure at the interface of the irradiated track and original wafer surface is attributed to the melt flow, different solidification temperatures of the pure Si and carbon-rich phases, and heterogeneous nucleation. The melt moves away from the center of the melt pool to the above-mentioned interface due to the surface tension gradient-driven flow known as Marangoni convection [40]. Since the solidification temperature of the carbon-rich phase is higher than that of the pure Si phase, the carbon-rich phase solidifies first via heterogeneous nucleation on the SiC substrate surface at the above-mentioned interface. As the temperature decreases further, liquid Si solidifies via heterogeneous nucleation at the surface of the solidified carbon-rich phase and tends to assume circular symmetry due to the surface tension force.

A cross-section of the irradiated track is shown in Fig. 8b. The maximum depth of the laser-generated groove, which depends on the process parameters such as the laser beam scanning speed, interaction time, laser beam power and shape, was measured to be 50 μm. The groove is formed partly due to the loss of Si by vaporization and partly due to the flowing away of the molten material from the laser beam center to the edge of the melt pool.

8. Energy dispersive spectroscopy (EDS) for elemental analysis

EDS was used to measure the atomic concentration of different species in CW Nd:YAG laser-treated sintered α-SiC sample at various distances from the laser beam center as shown in Fig. 9 highlighting the following result:

The atomic ratio of Si to C for the as-received SiC and after laser treatment in different environments are found to be $[Si/C]_{as\text{-}received} > [Si/C]_{argon} > [Si/C]_{nitrogen} > [Si/C]_{TMA+argon}$ at the beam center. These ratios are based on the amount of Si and C present in all the phases, such as unmelted SiC, free carbon, and silicon with dissolved carbon formed due to laser irradiation. The variation in the atomic ratio may be due to the formation of liquid silicon by any of the three mechanisms, i.e., thermal, doping, and chemical effects, during laser treatment in different environments and subsequent loss of silicon by vaporization. The thermal effect refers to the peritectic decomposition of SiC [2, 7] at high temperatures, while the doping effect involves the physical process of an atom being displaced by the dopant atom.

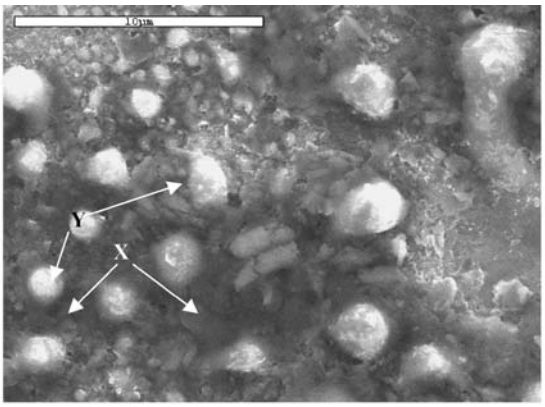

(a) Peripheral region of the irradiated track with different sizes of Si-rich globules (white spots) surrounded by carbon-rich (dark region) phases. High magnification of region C shown in Fig. 7b.

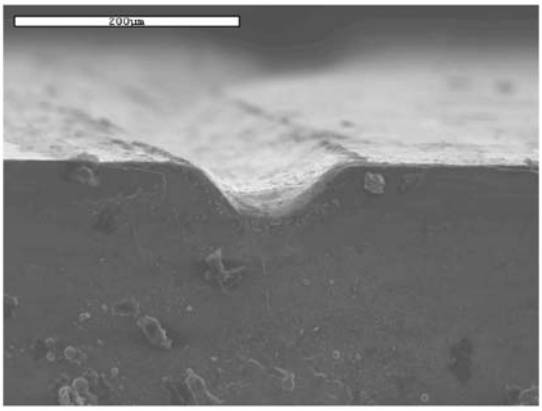

(b) Cross-section of the irradiated track showing the formation of a U-shaped trench at the beam center due to the loss of materials by vaporization and lateral flow of the molten materials away from the track center.

Figure 8 SEM micrographs of the laser argon-treated 4H-SiC wafer. Laser irradiation conditions are the same as in Fig. 7.

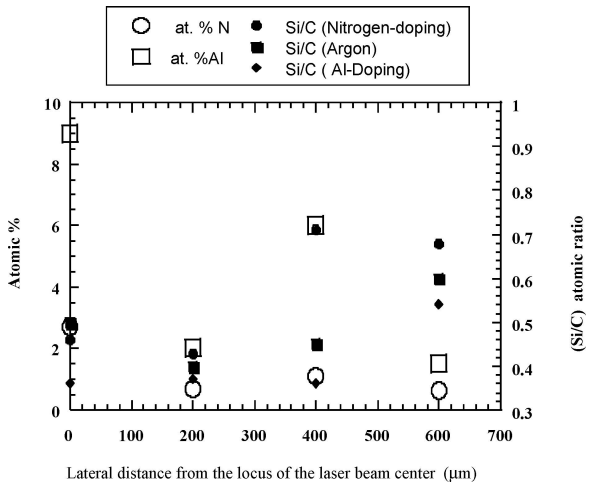

Figure 9 The average elemental concentration obtained by EDS for different species along the radius of the laser-irradiated tracks for the sintered α-SiC sample. Also illustrated is the measured Si/C ratio at different locations along the track.

The chemical effect refers to the mechanism in which the presence of dopant species in the irradiation environment weakens the Si–C bond and enhances the kinetics of the peritectic reaction in the forward direction. In the case of laser doping of SiC [28], Al is more reactive with SiC than nitrogen because the amount of Al is found to be higher than the amount of nitrogen (Fig. 9) at different lateral distances in the tracks produced by laser treatment in the presence of TMA and argon mixture and nitrogen, respectively. Due to these effects, different phases are formed in the laser-melted pool as discussed below. Reaction (i)-laser irradiation in argon environment (peritectic decomposition of SiC)

$$\mathrm{SiC} \overset{T>2700\mathrm{K}}{\longrightarrow} \mathrm{C} + \mathrm{Si(C)\,[liquid]} + \mathrm{SiC\,(unmelted)}$$

Reaction (ii)—laser irradiation in nitrogen environment leading to nitrogen doping

$$\mathrm{SiC} + \mathrm{N} \longrightarrow \mathrm{Si\text{-}C\text{-}N}_{(\text{doped phase})} + [\mathrm{C}]_{\text{doping effect}} + \left[\mathrm{C} + \mathrm{Si(C)}_{[\text{liquid}]} + \mathrm{SiC}_{(\text{unmelted})}\right]_{\text{peritectic reaction}}$$

Reaction (iii)—laser irradiation in argon and TMA mixture leading to aluminum doping

$$\mathrm{SiC} + \mathrm{Al} \longrightarrow \mathrm{Si\text{-}C\text{-}Al}_{(\text{doped phase})} + [\mathrm{Si}]_{\text{doping effect}} + \left[\mathrm{C} + \mathrm{Si(C)}_{[\text{liquid}]} + \mathrm{SiC}_{(\text{unmelted})}\right]_{\text{peritectic reaction}}$$

Reaction (i) may be the first step preceding each of the doping reactions (ii) and (iii) at high temperatures. Nitrogen displaces C to occupy the C sites and Al displaces Si to occupy the Si sites in the SiC lattice in reactions (ii) and (iii), respectively, because the atomic radii of Al and Si as well as N and C are similar. Therefore, the amount of free Si atoms formed in reaction (iii) is expected to be larger than that in reaction (ii), and hence more silicon is available in the liquid phase for vaporization in the case of Al doping than in the case of nitrogen doping. The melt pool is expected to lose more Si atoms than C atoms due to vaporization since Si vaporizes more readily than C. Accordingly, the Si/C ratio in the laser nitrogen-treated track is higher than the Si/C ratio in the tracks created in argon and TMA mixture. Another reason for this trend could be the chemical effect. Both ratios, $[\mathrm{Si/C}]_{\mathrm{nitrogen}}$ and $[\mathrm{Si/C}]_{\mathrm{TMA+argon}}$, are lower than that in the argon-treated tracks since no atomic replacement takes place in the SiC phase during laser argon treatment. The presence of the unmelted SiC phase as one of the products in reactions (i) through (iii) is attributed to the fast heating and rapid solidification in laser processing.

The results shown in Fig. 9 are in agreement with the XRD and the XPS results as reported in Fig. 3c and Table I, respectively. Since the irradiation environment does not affect the surface temperature (Fig. 1), one may conclude from the above-mentioned results that the dopant atoms affect the peritectic reaction kinetics and accelerate the formation of the nonequilibrium, conductive phases in laser-treated SiC substrates.

9. Electrical resistance conversion

The electric resistances (R_e) of CW Nd:YAG laser-generated 7 mm long and 1 mm wide tracks on a 2.5 mm thick sintered α-SiC sample are plotted as a function

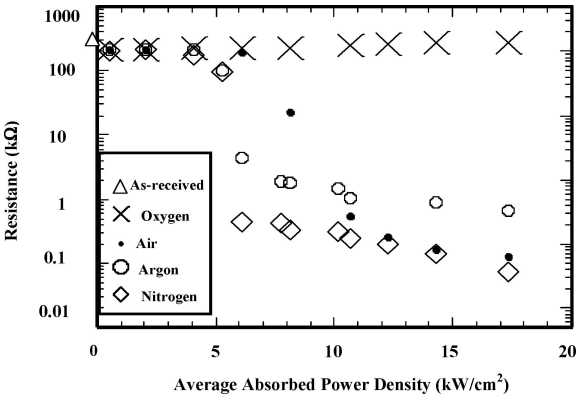

Figure 10 Electric resistances of 7 mm long and 1 mm wide laser-generated tracks on a sintered α-SiC substrate in different ambient gases as a function of the average absorbed power density. A CW Nd:YAG laser of beam spot diameter 1 mm and scanning speed 1 mm/s was used. The sample thickness was 2.5 mm. Gas pressure for nitrogen, argon, and oxygen was 0.1 MPa, and atmospheric pressure for air.

of the incident laser power density in Fig. 10. The laser irradiation experiments were carried out in argon, oxygen, and nitrogen environments at 0.1 MPa for each case and in air at atmospheric pressure. While the resistance increases slightly in laser oxygen-treated samples, it decreases significantly from 300 kΩ to 1, 0.12, and 0.07 kΩ in argon, air and nitrogen, respectively at the maximum conversion power density of 17 kW/cm^2. The maximum conversion power density is defined as the incident laser power density that reduces the electric resistance by a maximum amount. For different gases, there is a critical power density of the incident laser beam, I_c, below which the effect of the laser irradiation on the conversion of electric resistance is minimal. The value of I_c is lower for nitrogen than for argon, while I_c is higher for air than for argon. The decrease in the electric resistance upon irradiation in air is attributed to the competitive interactions of the nitrogen and oxygen contents of air with the SiC substrate. The increase in the electric resistance due to laser treatment in oxygen environment is attributed to the formation of a thin oxide layer at the substrate surface. The exact stoichiometry of the oxide film is not known at this time, but whether it is pure silicon oxide or silicon oxicarbide, the resistivity is expected to be higher than that of the original SiC sample and its magnitude will depend on the exact stoichiometry and degree of crystallinity of the film.

The results shown in Fig. 10 and Table II indicate that the resistance of the track produced in the TMA and argon mixture is lower than that of the track produced in only argon atmosphere. Similarly, the tracks generated in nitrogen environment exhibit substantially lower resistance than the as-received and laser argon-treated samples.

The decrease in the electric resistance of different SiC polytypes after laser irradiation is due to the heat effect of the laser beam and the dopant effect of nitrogen and Al in the SiC substrates. In laser argon-treated samples, the formation of carbon-rich phases, fine globular structures, and the appearance of new phases containing Si–Si and C=C bondings at the substrate surface as indicated by the XPS results reported in Table I and Fig. 5 lead to the decrease in electrical resistance. For samples irradiated in nitrogen and in the mixture of TMA and argon, the dopant effect of N and Al atoms, combined with the above-mentioned heat-induced morphological and compositional changes, decreases the electric resistance further. It should be noted that the n-type (nitrogen) and p-type (aluminum) dopants are expected to decrease and increase the electric resistances of the doped substrate respectively. In the case of sintered α-SiC, however, the electric resistances of two types of laser-treated tracks (one laser-treated in nitrogen and the other laser-treated in argon-TMA mixture) are almost the same (Table II), although the Al-content is significantly higher than the nitrogen content in these two laser-treated tracks (Fig. 9). This may be due to the higher energy required for aluminum dopant activation, since the ionization energy of shallow donors is 0.085–0.1 eV and 0.23–0.24 eV for nitrogen and aluminum dopants in 6H-SiC, respectively. This may also be due to the difference in the mobility of the majority carriers in the nitrogen-doped and the aluminum-doped silicon carbide [7]. For 4H-SiC samples, the resistances $R_{e,i}$ (Table III), where i = oxygen, argon and nitrogen denoting the surrounding gas during laser treatment and i = as-received implying the untreated sample, exhibit a trend similar to the case of sintered a-SiC (Fig. 10), i.e., $R_{e,\text{oxygen}} > R_{e,\text{as-received}} > R_{e,\text{argon}} > R_{e,\text{nitrogen}}$. The reasons for this decrease in the electric resistance of 4H-SiC are also similar to those discussed above for the sintered α-SiC samples.

However, due to the different optical properties of these two types of samples (Figs 1, 2a and b), different irradiation modes were used to induce electric resistance changes in each case. High absorption of the

TABLE II Electric resistance of sintered α-SiC samples irradiated in different environments. The laser irradiation was conducted using a CW Nd:YAG laser of beam spot diameter 1 mm and scanning speed = 1 mm/s. The average absorbed power density was 10 kW/cm^2 and the gas pressure was 0.1 MPa for argon and nitrogen and atmospheric pressure in the case of irradiation in air

Sample condition	Resistance (kΩ)
Untreated	300 ± 5
Laser-treated in oxygen	200 ± 5
Laser-treated in air	20 ± 0.15
Laser-treated in argon	1.5 ± 0.2
Laser-treated in nitrogen	0.30 ± 0.3
Laser-treated in argon-TMA mixture	0.25 ± 0.7

TABLE III Electric resistance of low-doped epilayer 4H-SiC wafer irradiated in different environments. Laser beam diameter = 1 mm, Q-switched mode, pulse repitition rate = 2 kHz, pulse width = 70 ns, pulse energy = 0.7 mJ, scanning speed = 0.8 mm/s. gas pressure = 0.1 MPa for oxygen, argon and nitrogen and atmospheric pressure in the case of irradiation in air.

Sample condition	Resistance (kΩ)
Untreated	$23 \times 10^4 \pm 5$
Laser-treated in argon	1.2 ± 0.25
Laser-treated in nitrogen	0.25 ± 0.05
Laser-treated in air	$2.5 \times 102 \pm 3$
Laser treated in oxygen	$30 \times 104 \pm 7$
Laser-treated in argon followed by nitrogen	1.1 ± 0.15
Laser-treated in nitrogen followed by argon	0.85 ± 0.2

polycrystalline 6H-SiC samples at $\lambda = 1064$ nm suggested that the continuous wave (CW) laser irradiation is sufficient to cause electric resistance conversion in such samples. Lower absorption of the 4H-SiC low-doped epilayer and CVD β-SiC samples at this wavelength necessitates the use of Q-switched laser pulses to achieve conversion in electric resistance. Nanosecond pulses in the Q-switched mode allow to irradiate the samples at higher power densities than the CW laser and hence deposit more energy per unit area per unit time overcoming the effect of lower absorptivity of the sample. It should be noted that the electric resistance of 0.20 mm thick 4H-SiC wafer remained unaffected by the CW laser irradiation at powers less than 100 W, while the sample cracked along the irradiated track at higher powers (>100 W). Although the incident power density is much higher in the Q-switched case, longer laser-substrate interaction time during CW irradiation (*i.e.*, 1 s at $P = 120$ W in the case of CW irradiation versus 6 ms at the pulse repetition rate = 1 kHz, pulse energy = 0.8 mJ and pulse width = 60 ns in the Q-switched mode) resulted in a sufficient thermal stress in the sample to initiate a crack along the laser-treated track.

The double gas exposure experiments, *i.e.*, laser irradiation of the same substrate in two different environments - nitrogen followed by argon and vice versa (Table III), alters the electric resistance in the following order: $R_{e,\text{nitrogen}} < R_{e,\text{nitrogen-argon}} < R_{e,\text{argon-nirogen}} < R_{e,\text{argon}}$. These results imply that less nitrogen is incorporated into the substrate in the double gas exposures than in the single nitrogen gas exposure. The reason for this trend could be explained using the site competition principle which states that p-type doping into SiC lattice is enhanced by increasing the C/Si ratio in the gaseous precursors during the SiC *in situ* doping by the chemical vapor deposition (CVD) method [13]. Similarly, large Si/C ratio in the gaseous precursors was reported to enhance the n-type doping in the same method. By analogy, the incorporation of nitrogen atoms into the laser-induced carbon-rich SiC phase could be energetically less favorable than nitrogen doping into as-received SiC. The variation in the electric resistance observed in the double gas exposure experiments could also be related to nitrogen out-diffusion that might occur upon laser irradiation for the second time in argon. The out-diffusion will decrease the number of the effective nitrogen atoms inside the SiC lattice and hence will increase the resistance.

10. Conclusions

The absorption of the sintered 6H-SiC is higher than that of the 4H-SiC low-doped epilayer and the CVD β-SiC at $\lambda = 1064$ nm. Due to this, a continuous wave laser is used for processing the sintered 6H–SiC sample, while a Q-switched pulsed laser is used for the 4H-SiC wafer. The critical energy required to achieve conversion in electric resistance coincides with that required to increase the silicon carbide surface temperature to its peritectic reaction. Different analytical (XPS, XRD, SEM and EDS) studies of the laser-treated tracks reveal the presence of carbon-rich phases. The presence of both nitrogen and aluminum species is also detected in the tracks irradiated in nitrogen and in a mixture of TMA and argon, respectively. The conversion in electric resistance after laser treatment in inert gas (argon) is mainly due to a thermal effect, *i.e.*, laser heating causing peritectic reaction in SiC. In the case of irradiation in nitrogen and in a mixture of TMA and argon, the conversion is attributed partly to the thermal effect and partly to the incorporation of nitrogen and aluminum as dopants into the SiC matrix. The creation of conductive tracks on insulating silicon carbide substrates and the incorporation of dopant atoms into the SiC matrix by laser treatment are important in using the laser direct-write technique for SiC-based electronic and optoelectronic device fabrication.

References

1. G. PENSEL and A. D. CHOYKE, *Physica B* **185** (1993) 264.
2. H. PIERSON, "Handbook of Refractory Carbides and Nitrides" (1st. ed., Noyess publications, New Jersy, 1996), p. 188.
3. J. A. POWELL, D. J. LARKIN, L. G. MATUS, W. J. CHOYKE, J. L. BRADSHAW, L. HENDERSON, M. YOGANATHAN, J. YANG and P. PIROUZ, *Appl. Phys. Lett.* **56**(14) (1990) 1353.
4. S. J. PEARTON, "Processing of Wide Band Gap Semiconductors" (1st ed., William Andrew publishing, New York, 2000), p. 182, 183.
5. J. SINGH, "Semiconductor Devices: Basic Principles" (1st ed. John Wiley & Sons, New York, 2001) p. 358.
6. L. M. PORTER and R. F. DAVIS, *Mater. Sci. Eng. B* **34** (1995) 83.
7. M. E. LEVINSHTEIN, S. L. RUMAYANTSEV and M. S. SHUR, "Properties of Advanced Semiconductor Materials" (1st ed. John Wiley and Sons, New York, 2001) p. 93–147.
8. O. MADELUNG, "Data in Science and Technology: Semiconductors Group IV Elements and III-V Compounds" (Springer-Verlag, Berlin, 1991) p. 101.
9. C. H. CARTER, JR., V. F. TSVETKOV, R. C. GLASS, D. HENSHALL, M. BRADY, ST. G. MULLER, O. KORDINA, K. IRVINE, J. A. EDMOND, H. S. KONG, R. SINGH, S. T. ALLEN and J. W. PALMOUR, *Mat. Sci. and Eng. B* **61/62** (1999) p. 1.
10. G. L. HARRIS, "Properties of Silicon Carbide", Emmys DATAREVIEW series No. 13 (inspec publication, Exeter, 1995) p. 153.
11. W. J. CHOYKE, H. MATSUNAMII and G. PENSEL, "Silicon Carbide-A review of Fundamental Questions and Applications to Current Device Technology" (Wiley- VCH, Berlin, 1997).
12. G. GARDINARU, T. S. SUDARSHAN, S. A. GARDINARU, W. MITCHEL and H. M. HOBOGOOD, *Appl. Phys. Lett.* **70** (1997) 735.
13. P. G. NEUDECK, *SiC Technology* in "VLSI Handbook", edited by W. K. Chen, Ed. Boca Raton (CRC press and IEEE press, Florida, 2000) p. 6.1.
14. T. TROFFER, M. SCHDT, T. FRANK, H. ITOH, G. PENSEL, J. HEINDI, H. P. STRUNK and M. MAIER, *Phys. Status. Solidi A.* **162** (1997) 277.
15. E. M. HANDY, M. V. ROW, O. W. HOLLAND, P. H. CHI, K. A. JONES, M. A. DERENGE, R. D. VISPUTE and T. VENKATESEN, *J. Electron. Mater.* **29** (2000) 1340.
16. M. A. CPANO, S. RYU, M. R MELLOCH, J. A COOPER and M. R BUSS, *J. Electron. Mater.* **27** (1998) 370.
17. H. ITOH, T. TROFFER and G. PENSL, *Materials Science Forum* **264/268** (1998) 685.
18. G. PENSL, V. AFANS, M. BASSIER, T. FRANK and M. LAUBE, *Mater. Sci. Forum* **338/342** (2000) 831.
19. L. A. CHRISTEL and J. F. GIBBONS, *J. Appl. Phys.* **52** (1981) 5050.
20. N. R. QUICK, in Proceedings of International Symposium on Novel Techniques in Synthesis and Processing of Advanced

Materials, edited by J. Singh and S. M. Copley (TMS, Warrendale, PA, 1994) p. 419.
21. N. R. QUICK, in Proceedings of the International Conference on Lasers' 94 edited by V. J. Corcoran and T. A Goldman, (STS press, McLean, Virginia, 1995) p. 696.
22. N. R. QUICK, "Converting Ceramic Materials to Electrical Conductor and Semiconductors," US Patent no. 5, p. 145, 741 (Sept. 1992).
23. N. R. QUICK, "Laser Synthesized Ceramic Electronic Devices and Circuits," (US Patent No 5837607, Nov. 1998).
24. N. R. QUICK, "Laser Synthesized Ceramic Electronic Devices Method of Making," (US Patent No 6025609, Feb. 2000).
25. N. R. QUICK, "Method for Making Laser Synthesized Ceramic Electronic Devices and Circuits," (US Patent No 6054375, April 2000).
26. D. K. SENGUPTA, N. R. QUICK and A. KAR, *J. Laser Applications* **13** (2001) 26.
27. D. K. SENGUPTA, N. R. QUICK and A. KAR, *Laser Synthesis of Ohmic Contacts in Silicon Carbide Having Schottky Diode Characteristics Before Laser Treatment*, presented at "Int. Cong. on Appl. of Lasers and Electro-Optics" ICALEO, Jacksonville, Florida USA 2001.
28. I. A. SALAMA, N. R. QUICK and A. KAR, "*Laser Doping of Silicon Carbide substrates*", *J. Elec. Mats.* **31** (2002) 200.
29. W. J SPITZER, A. KLEINMAN and D. J. WALSH, *Phys. Rev.* **113** (1959) 127.
30. W. M. STEEN, "Laser Material Processing" 2nd ed., (Springer-Verlag publications, London, 1998). p 109.
31. J. XIE and A. KAR, in Proceedings of the International Conference on Lasers' 95, edited by J. Mazumder, A. Matsunawa, and C. Magnusson. ICALEO Proceedings (LIA publications, Orlando, Fl.,1995).
32. X-ray powder diffraction data for Silicon Carbide, PDF # 42–1360.
33. X-ray powder diffraction data for Silicon, PDF # 41–1111.
34. X-ray powder diffraction data for 2H-Graphite, PDF # 41–1487.
35. X-ray powder diffraction data of Nitrogen, PDF # 23–1294.
36. X-ray powder diffraction data for Silicon Nitride, PDF # 33–1160.
37. Y. V . FATTAKHOV, R. M. BAYAZITOV, I. B. KHAIBULLIN and T. N. L'VOVA, "High Power laser- Science and Engineering" (Kluwer academic publishers, Netherland, 1996) p. 533.
38. V. I. EMEL YANOV, *Laser Physics* **2** (1992) 389.
39. J. DORWAT , G. DE MARIA and M. G. INGRAM, *J. Chem. Phys.* **29** (1958) 1015.
40. T. FUHRICH, P. BERGER and H. HUGEL, *J. Laser Appl.* **13** (2001) 178.

Received 27 February 2004
and accepted 24 March 2005